Enantiomers separation by simulated moving bed chromatography Non-instantaneous equilibrium at the solid–fluid interface

D.C.S. Azevedo[1], L.S. Pais, A.E. Rodrigues*

Laboratory of Separation and Reaction Engineering, School of Engineering, University of Porto Rua dos Bragas, 4099 Porto Codex, Portugal

Abstract

The simulated moving bed (SMB) technology, first conceived for large bulk-scale separations in the petrochemical industry, has found increasingly new applications in the pharmaceutical industry. Among these, the separation of fine chemicals has been the subject of considerable study and research. This work presents the modeling, simulation and design of the operation of a SMB plant in order to separate a binary chiral mixture. The usual assumption of instantaneous equilibrium at the solid–fluid interface is questioned and a first-order kinetics of adsorption is taken into account. The cases of linear, Langmuir and modified Langmuir equilibria are studied. The equivalent true moving bed (TMB) model was used assuming axial dispersion for the fluid flow and plug flow for the solid-phase flow. Intraparticle diffusion was described by a linear driving force (LDF) approximation. Simulation results indicate that, under certain conditions, equilibrium is not actually reached at the adsorbent surface. This leads to different unit performances, in terms of product purities and recoveries, as compared to those predicted assuming instantaneous equilibrium. Moreover, SMB units may be improperly designed by the usual methods (flow-rate ratio separation regions) if non-equilibrium effects are overlooked. © 1999 Elsevier Science B.V. All rights reserved.

Keywords: Enantiomer separation; Simulated moving bed chromatography; Adsorption kinetics; Non-linear chromatography; Non-equilibrium effects

1. Introduction

The simulated moving bed (SMB) technology was first conceived for large bulk separations in the petrochemical industry. Since it was patented in the early 1960s by Universal Oil Products (UOP) [1–5], it has found increasingly new areas of application with special emphasis on fine chemicals industry [6–10]. A separation of particular interest to the

pharmaceutical industry is that of chiral mixtures. It is well known that some optical isomers may exhibit completely different, and even opposing, pharmacological effects. As a consequence, new chiral separation methods are being proposed nowadays to produce single enantiomeric forms of chiral drugs [11–15]. SMB chiral chromatography is a promising technique for the industrial production of single enantiomeric drugs able to compete with up to now other dominating methods such as elution batch chromatography, diastereoisomeric crystallization or asymmetric synthesis [16]. SMB is essentially a binary mixture separation technique, hence particularly suitable for racemic resolution.

The SMB operating principle consists in simulat-

ing fluid counter-current motion relative to a solid adsorbent by means of an appropriate flow switching scheme. As may be seen in Fig. 1, the adsorbent is equally divided into a number of m fixed beds. The inlet streams are the feed, which contains the binary mixture to be separated and the eluent/desorbent, which is the adsorbent regeneration agent. The outlet streams are the extract, which should be enriched with the more strongly adsorbed component (A), and the raffinate, which should be enriched with the weakly adsorbed component (B). These inlet/outlet ports are shifted one bed ahead in the direction of the fluid flow at regular time intervals (the rotation period). This arrangement is equivalent to an actual movement of the solid adsorbent relative to the fluid flow with fixed inlet/outlet ports (see Fig. 1). This equivalent representation, the true moving-bed

(TMB), is an idealized model which has been frequently used for SMB modeling purposes [17] due to the required less costly computational effort and to the possibility of direct assessment of the steady-state performance.

The key to a successful chiral separation by SMB chromatography resides in two basic aspects: (1) correct choice of operating conditions and (2) correct choice of the stationary phase. As for the first aspect, several techniques have been proposed [18–21] to design appropriate SMB operating conditions which enhance purities, recoveries, productivity and minimize solvent requirements. Designed for high productivity separations, SMB units usually operate at high feed concentrations leading to non-linear competitive adsorption behaviors. Therefore, modeling and simulation tools are of crucial importance before
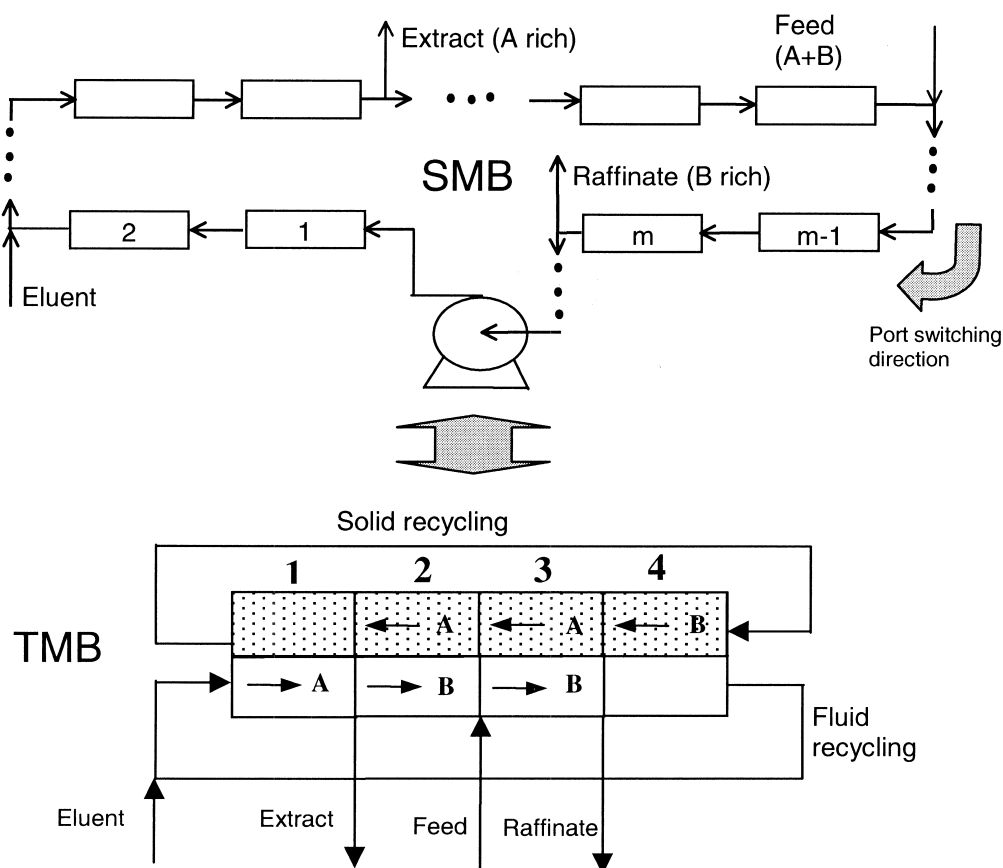

Fig. 1. Representation of a simulated moving bed (SMB) and the equivalent true moving bed (TMB) with flow restrictions.

D.C.S. Azevedo et al. / J. Chromatogr. A 865 (1999) 187–200

189

running the system. This requires a knowledge of some basic information on equilibrium and kinetic parameters.

As for the second aspect previously mentioned, several stationary phases with chiral recognition properties have been proposed in the literature [22–27]. For the great majority of them, the determination of precise multicomponent competitive adsorption isotherms is a crucial aspect. Although the mechanism of chiral recognition is still unclear, the presence of non-chiral and chiral adsorption sites has been frequently reported [22,26,27] and accounted for by a modified Langmuir isotherm as expressed in Eq. (1):

$$q_{si}^* = K_i C_i + \frac{b_i q_m C_i}{1 + b_A C_A + b_B C_B}; \quad i = A, B \tag{1}$$

The illustrative example examined in this work for such isotherm is that of a microcrystalline cellulose triacetate (CTA) used as a SMB stationary phase for the separation of a chiral epoxide. The use of this adsorbent in its swollen state has been reported in the literature [28–31] for various chiral separations. It seems that, unlike common stationary phases, adsorption on microcrystalline CTA is more influenced by steric effects than by the chemical nature of the interaction between the chiral species and the stationary phase substituents [16]. When steric hindrances are present, it is very likely that non-equilibrium adsorption/desorption effects take place. This has been pointed out as the cause of the observed mismatch between predicted and experimental results by some authors [16,32,33]. Whitley et al. [32] examined the effects of non-equilibrium adsorption/desorption on breakthrough and elution curves in affinity/perfusion chromatographic systems with Langmuir equilibrium isotherms. They concluded that, in analytical and preparative scale chromatography, non-equilibrium at the solid–fluid interface is responsible for such symptoms as symmetric and asymmetric broadening, apparent loss of capacity, loss of coherence and deviations from the interference patterns of local equilibrium systems. Rodrigues et al. [33] also addressed this matter for large pore supports used in chromatographic bioseparations under linear equilibria. They examined the influence of the kinetics of adsorption in the height

equivalent to a theoretical plate (HETP) and proposed criteria in order to verify to which extent non-equilibrium effects are important as compared with the other mass transfer/dispersion phenomena. LeVan [34] stresses that one of the key areas of advance in adsorption fundamentals is the fully correct understanding of adsorption equilibrium and rate behavior and the incorporation of the derived accurate relations into the mathematical models used for process description.

This work intends to contribute to the effort of a more comprehensive understanding of non-instantaneous local equilibria, applied to the operation of a simulated moving bed, by proposing a first-order kinetics of adsorption for linear and non-linear isotherms and by examining the implications of this assumption on SMB modeling and design.

2. Theory

2.1. Modeling kinetics of adsorption/desorption at the solid–fluid interface

If a homogeneous adsorbent particle is submitted to a concentration C at its surface, the LDF approximation states that the rate of sorbate uptake may be written as:

$$r_{diff} = k_p(q_s - \bar{q}) \tag{2}$$

where $\bar{q}$ is the adsorbed phase concentration averaged over the particle volume, k_p is the homogeneous mass transfer rate constant and q_s is the concentration at the particle surface. The hypothesis of instantaneous equilibrium at the solid surface is very often accepted and q_s is related to the fluid phase concentration C by means of the equilibrium isotherm equation.

However, equilibrium is very frequently not attained instantaneously but follows a given kinetics as shown in Fig. 2. For a linear equilibrium isotherm, if a kinetics of sorption of first-order is assumed, the rate of adsorption can be expressed as:

$$r_{ads} = k_1 C - k_2 q_s = k_2(KC - q_s) \tag{3}$$

where k_1 and k_2 represent the adsorption and desorption rate constants, respectively, and K is the ad-
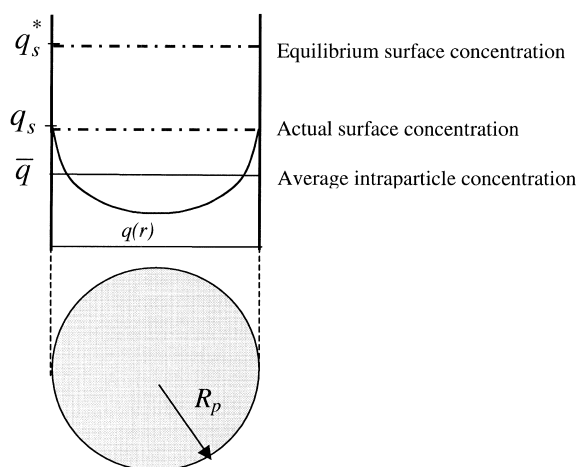
Fig. 2. Representation of an adsorbent particle with intraparticle mass transport and non-equilibrium adsorption effects on its surface.

sorption equilibrium constant. If a mixture of species A (more strongly adsorbed component) and B (less adsorbed component) is in contact with the adsorbent, Eq. (3) is valid for each of the components.

For a Langmuir equilibrium isotherm, the first-order kinetic law for the rate of adsorption would be expressed as:

$$r_{adsA} = k_1 C_A (q_m - q_{sA} - q_{sB}) - k_2 q_{sA}$$
$$= k_2 [b_A C_A (q_m - q_{sA} - q_{sB}) - q_{sA}] \qquad (4)$$

where b is a Langmuir isotherm parameter and q_m is the maximum adsorbent capacity. The subscripts A and B denote the chemical species involved.

For adsorbents with chiral selectivity, a combined linear+Langmuir isotherm has been frequently proposed in the literature [22,26,27]. In this case, the rate of adsorption would be the sum of the rates of adsorption for non-chiral and chiral sites denoted by the superscripts "NC" and "C", respectively.

$$r_{adsA} = k_2^{NC} (K_A C_A - q_{sA}^{NC})$$
$$+ k_2^C [b_A C_A (q_m^C - q_{sA}^C - q_{sB}^C) - q_{sA}^C] \qquad (5)$$

Assuming that the non-chiral sites do not exhibit adsorption kinetics, the first term on the right-hand side of Eq. (5) is equal to zero. Consequently, $q_{sA}^C = q_{sA} - K_A C_A$ and $q_{sB}^C = q_{sB} - K_B C_B$. Eq. (5) may be written as:

$$r_{adsA} = k_2 [b_A C_A (q_m - q_{sB} + K_B C_B)$$
$$+ (1 + b_A C_A)(K_A C_A - q_{sA})] \qquad (6)$$

For modeling purposes of adsorptive processes, the concentration at the adsorbent surface q_{si} ($i = A, B$) must be related to the other variables of the problem. This may be done by assuming that the rate of adsorption, as given in Eqs. (3), (4) and (6), is equal to the rate of intraparticle mass transfer as given in Eq. (2). By doing so, and solving the remaining equations for q_{si}, one gets the following equations.

For linear equilibrium:

$$q_{si} = \frac{K_i C_i + \Omega \bar{q}_i}{1 + \Omega}; \quad i = A \ or \ B \qquad (7)$$

For Langmuir equilibrium:

$$q_{sA} = \frac{b_A C_A (q_m - q_{sB}) + \Omega \bar{q}_A}{1 + b_A C_A + \Omega} \qquad (8)$$

$$q_{sB} = \frac{b_B C_B (q_m - q_{sA}) + \Omega \bar{q}_B}{1 + b_B C_B + \Omega} \qquad (9)$$

For linear+Langmuir isotherm:

$$q_{sA} =$$
$$\frac{b_A C_A (q_m - q_{sB} + K_B C_B) + (1 + b_A C_A) K_A C_A + \Omega \bar{q}_A}{1 + b_A C_A + \Omega}$$
$$(10)$$

$$q_{sB} =$$
$$\frac{b_B C_B (q_m - q_{sA} + K_A C_A) + (1 + b_B C_B) K_B C_B + \Omega \bar{q}_B}{1 + b_B C_B + \Omega}$$
$$(11)$$

Ω is the ratio between the mass transfer rate constant k_p and the adsorption/desorption rate constant k_2. From Eqs. (7)–(11), the extreme cases are easily verified. If $k_2 << k_p$, adsorption kinetics is the limiting rate mechanism; $1/\Omega$ tends to zero and $q_{si} \approx \bar{q}_i$. On the other hand, if $k_p << k_2$, equilibrium at the surface is reached locally; Ω tends to zero and $q_{si} \approx q_{si}^*$, as expressed by the corresponding isotherm. When both sorption and intraparticle mass transfer rates have comparable magnitude, q_s, as given from

Eq. (7)–(11) may be written as an algebraic equation together with the mass balance equations of the adsorptive process model.

The modeling of a simulated moving bed may follow two strategies [17]: (1) it may be represented by the equivalent TMB as depicted in Fig. 1. In this case, each of the four sections is treated as a counter-current bed and the solid moves with a velocity U_S which is equal to the actual bed length (L_b) divided by the switching time (t^*). The steady state is a definite condition with stationary internal profiles and unchanging product (extract and raffinate) concentrations. (2) The SMB may be represented as the actual physical configuration (SMB), that is, a group of fixed beds connected in series with moving boundary conditions at regular time intervals. The steady state, in this case, is a periodic condition with moving internal profiles that follow a constant pattern. The product concentration also varies within a period, although the cycle averages are constant. The equivalence between these two representations has been demonstrated [17] for the subdivision of at least two columns per section. The equivalent TMB model was used in this work since it saves computational time and permits the direct assessment of steady-state performance.

2.2. Equivalent true moving-bed (TMB) model

A steady-state model to describe a four-zone SMB unit (see Fig. 1) for a binary mixture separation was proposed based on the analogous true counter-current moving bed (TMB). The assumption of non-instantaneous equilibrium was taken into account and the LDF approximation was used to describe intraparticle mass transfer. Axial dispersion was considered for the fluid phase whereas plug flow was assumed for the solid-phase. Model equations for a component i at a section j of the TMB are as follows.

$$\frac{\gamma_j}{\text{Pe}_j} \cdot \frac{d^2 C_{i,j}}{dx^2} - \gamma_j \cdot \frac{dC_{i,j}}{dx} - \nu \alpha_{i,j}(q_{si,j} - \bar{q}_{i,j}) = 0 \quad (12)$$

$$\frac{d\bar{q}_{i,j}}{dx} + \alpha_{i,j}(q_{si,j} - \bar{q}_{i,j}) = 0 \quad (13)$$

$$q_{si,j} = f_{\text{non-eq}}(C_{A,j}, C_{B,j}, \bar{q}_{A,j}, \bar{q}_{B,j}) \quad (14)$$

At $x = 0$

$$C_{i,j}^{\text{in}} = C_{i,j}(0) - \frac{1}{\text{Pe}_j} \left. \frac{dC_{i,j}}{dx} \right|_{x=0} \quad (15)$$

At $x = 1$

$$\left. \frac{dC_{i,j}}{dx} \right|_{x=0} = 0 \quad (16)$$

$$\bar{q}_{i,j}(1) = \bar{q}_{i,j+1}(0) \quad (17)$$

where $x = z/L_j$, $i = $ A or B and $j = 1, 2, 3, 4$

The parameters present in Eqs. (12) and (13) are defined as follows:

$$\text{Pe}_j = \frac{U_{Fj} L_j}{D_{axj}} \quad (18)$$

$$\nu = \frac{(1 - \epsilon)}{\epsilon} \quad (19)$$

$$\gamma_j = \frac{U_{Fj}}{U_S} \quad (20)$$

$$\alpha_j = k_p \frac{L_j}{U_S} \quad (21)$$

$$\Omega = \frac{k_p}{k_2} \quad (22)$$

The concentration in the inlet of each section, $C_{i,j}^{\text{in}}$, may be calculated from the mass balances in the four nodes of the SMB according to Eqs. (23)–(26).

Eluent node:

$$C_{i,1}^{\text{in}} = \frac{Q_4 C_{i,4}(1)}{Q_1} \quad (23)$$

Extract node:

$$C_{i,2}^{\text{in}} = C_{i,1}(1) \quad (24)$$

Feed node:

$$C_{i,3}^{\text{in}} = \frac{Q_F C_{F,i} + Q_2 C_{i,2}(1)}{Q_3} \quad (25)$$

Raffinate node:

$$C_{i,4}^{\text{in}} = C_{i,3}(1) \quad (26)$$

2.3. Prediction of separation regions and process performance

It has been said before that one of the keys to a successful SMB separation is the correct design of its operating conditions. For separation of a binary mixture to occur, each of the four sections of the SMB must perform a certain role. If a binary mixture of A (more strongly adsorbed component) and B (more weakly adsorbed component) is fed in a SMB, A will only move towards the extract port and B to the raffinate port if certain flow constraints are met. Next, these conditions will be stated bearing in mind the analogous representation of a true moving bed (see Fig. 1b).

Section 1 is the adsorbent regeneration zone. The more retained component, A, must be displaced by the eluent (solvent) to the fluid phase. Therefore, the net flow of A must be that of the fluid phase. In section 2, between extract and feed nodes, desorption of the weakly adsorbed component, B, happens. The net flux of B must be that of the fluid phase. Section 3 is where A is adsorbed. It must, then, move with the solid-phase. In section 4, the solvent is regenerated and the less retained component, B, is adsorbed. The net flux of B must be that of the solid-phase. These flow constraints may be expressed as the following:

$$\frac{Q_1 C_{A,1}}{Q_S \bar{q}_{A,1}} > 1 \tag{27}$$

$$\frac{Q_2 C_{B,2}}{Q_S \bar{q}_{B,2}} > 1; \quad \frac{Q_2 C_{A,2}}{Q_S \bar{q}_{A,2}} < 1 \tag{28}$$

$$\frac{Q_3 C_{B,3}}{Q_S \bar{q}_{B,3}} > 1; \quad \frac{Q_3 C_{A,3}}{Q_S \bar{q}_{A,3}} < 1 \tag{29}$$

$$\frac{Q_4 C_{B,4}}{Q_S \bar{q}_{B,4}} < 1 \tag{30}$$

The left hand term in the inequalities above may be re-written as:

$$\Gamma_{i,j} = \gamma_j \nu \cdot \frac{C_{i,j}}{\bar{q}_{i,j}} \tag{31}$$

From this point on, the term ''optimization'' will be used to designate the procedure of determining the finite group of flow-rate ratios γ_1, γ_2, γ_3, and γ_4

that satisfies Eqs. (27)–(30). In the frame of equilibrium theory, optimization requires only the knowledge of equilibrium data and has already been shown by Mazzotti et al. [19].

When kinetic effects are taken into account, the flow-rate ratios which enhance separation may only be accessed through numerical simulation of the corresponding steady-state SMB performance. Moreover, performance criteria (e.g., minimum required purities, recoveries, etc.) have to be defined since complete separation (100% extract/raffinate purity) is not achieved. In this work, minimum extract and raffinate purity of 99% was chosen as the criteria to define the region of separation in terms of flow-rate ratios. The constraint on section 4 together with residence time considerations were used to define arbitrarily the rotation period and recycle flow-rate to be considered in the optimization procedure. Then, for a given value of γ_1, in accordance with Eq. (27), the region of separation in a $\gamma_2 \times \gamma_3$ plane was determined by simulation using the steady-state TMB model.

2.4. Numerical solution of model equations

The TMB model as expressed in Eqs. (12)–(25) was solved using the public domain solvers COL-NEW [35] in the case of linear equilibrium isotherms and COLDAE [36] for the non-linear cases. The simulations required for optimization purposes were also performed with the aid of these solvers. Both COLNEW and COLDAE solve boundary-value problems for ordinary differential equations, the latter with constraints as given by the non-linear algebraic equations. The solution is approximated through collocation at Gaussian points; a Runge–Kutta monomial solution representation is utilized. In this work, the non-linear case required a much greater computational effort with stricter running parameters. Whereas for the linear case, 15 subdivisions per zone with two collocation points in each were enough for the steady-state calculations, the modified Langmuir case required 40 to 50 intervals per section with two collocation points in each. Moreover, the numerical solution given by COL-NEW ran in less than a minute with a Pentium II 300 MHz processor and the one COLDAE solution took around 1 h using the same machine.

3. Results and discussion

In order to study the non-equilibrium adsorption effects for linear isotherms, the classical case of fructose–glucose separation was chosen. Although there is no experimental evidence that such effects influence this system, it was selected as an illustrative example. Data from Leão et al. [37] were used and are shown in Table 1. Four different cases were simulated by varying the adsorption kinetic constant so as to obtain the values $\Omega = 0$, 0.1, 1, 10. The steady-state internal profiles obtained in each of these cases are shown in Fig. 3. For the cases of $\Omega = 0.1$ and 1, equilibrium is not actually reached at the solid surface. For $\Omega = 10$, there is virtually no separation at all. This may be caused by the strong resistance to adsorption equilibrium, which may have resulted in a violation of the constraints on the permissable solid/fluid flow-rate ratios. This point will be detailed in the results of the design procedure.

Note that, if q_s as given from Eq. (7) is inserted into the transfer term $k_p(q_{si,j} - \bar{q}_{i,j})$ present in the model Eqs. (12) and (13), the transfer term becomes:

$$k_p = \left(\frac{K_i C_{i,j} + \Omega \bar{q}_{i,j}}{1 + \Omega} - \bar{q}_{i,j} \right)$$

$$= \frac{k_p}{1 + \Omega} \cdot (K_i C_{i,j} - \bar{q}_{i,j}) = k_p'(q_{si,j}^* - \bar{q}_{i,j}) \qquad (32)$$

Eq. (32) is the transfer term written for instantaneous equilibrium at the adsorbent surface with a modified (smaller) mass transfer coefficient k_p'. Therefore, non-equilibrium effects on linear systems act only as an additional resistance to intraparticle mass transfer, but the clear distinction of both phenomena (kinetics of adsorption and mass transfer)

in process modeling enables us to address the effects of such variables as particle size and temperature. These variables affect the adsorption and mass transfer rate constants in diverse ways.

For the non-linear equilibrium isotherms, the case of SMB separation of a chiral epoxide using a microcrystalline cellulose triacetate was chosen to illustrate non-equilibrium effects. For this stationary phase, Pais et al. [16] have reported the experimental measurement of a modified Langmuir isotherm as expressed in Eq. (1) with $K = 1.35$; $q_m = 7.32$ g/l; $b_A = 0.163$ l/g and $b_B = 0.087$ l/g. The operation of a SMB with two columns per section was simulated using the operating conditions as given in Table 2.

Fig. 4 shows the simulated steady-state internal profiles obtained for different values of Ω. In all four examples, the concentration at the surface of the adsorbent particles (continuous curves) is about the same as the mean solid concentration (dashed curves) since the mass transfer rate constant is considerably high (24 min^{-1}). Nevertheless, as the resistance to equilibrium attainment increases (increasing values of Ω), the product purities are greatly affected, even for small values of Ω. Broader profiles are observed with increasing Ω not only in the solid-phase, but also in the fluid phase (not shown) with corresponding product contamination. As Ω increases, the concentration at the surface of the particle should deviate from the concentration that would be in equilibrium with the fluid phase concentration $C_{i,j}$. This is also shown in Fig. 4 by the graphs beside each profile. They show the relative errors in sections 2 and 3 for both species A and B. The relative error is defined as $100*(q_{si}^* - q_{si})/q_{si,k}^\infty$, where $q_{si,k}^\infty$ is defined as the adsorbed quantity of species i in equilibrium with the plateau concentration in zone k for $\alpha \to 64$ and $\Omega = 0$ (if $i = A$, $k = 2$; if $i = B$, $k = 3$).

Table 1
SMB setup for simulations of glucose–fructose separation

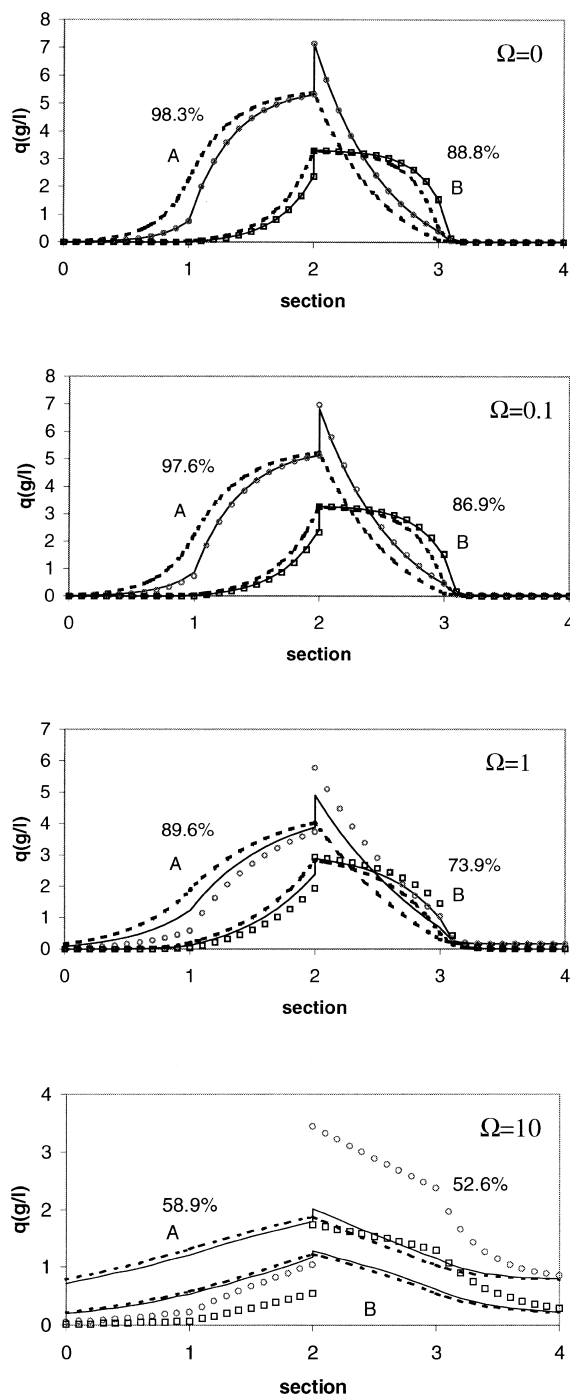| Model parameters	Operating conditions	Columns
Pe = 2000	$T = 20°C$	$D_b = 2.6$ cm
$k_p = 0.645$ min^{-1} (fructose)	Feed concentration = 30 g/l each	$L_b = 11.5$ cm
$k_p = 1.226$ min^{-1} (glucose)	$t^* = 3.3$ min	Configuration: 3-3-3-3
$K = 0.635$ (fructose)	$Q_{Rec} = 8.55$ ml/min	Zone length = 34.5 cm
$K = 0.314$ (glucose)	$Q_E = 20$ ml/min	
$\Omega = 0$, 0.1, 1, 10	$Q_X = 16.339$ ml/min	
$\nu = 1.5$	$Q_{FEED} = 0.740$ ml/min	

Fig. 3. Steady-state internal profiles for fructose (A) and glucose (B) under different non-equilibrium adsorption effects. The dashed curves stand for the mean solid-phase concentration, $\bar{q}$; the continuous curves stand for surface concentration, q_s and the points stand for equilibrium surface concentration, q_s^*.

To verify the influence of adsorbent particle size, the same case as described in Table 2 was simulated assuming a particle size twice as large. If the particle diameter is doubled, the intraparticle mass transfer becomes four-times as small as the original value. The number of mass transfer units will go down to 40. The corresponding simulations of SMB performance with the same setup as described in Table 2 is shown in Fig. 5. In all graphs, the difference between the concentration at the particle surface and the mean intraparticle concentration is noticeable. With increasing Ω, the difference between the concentration at the particle surface and the theoretical concentration in equilibrium with the fluid phase also becomes distinct.

The optimization procedure as described in the previous section was performed for both the linear and the non-linear cases. In the linear case, the search for adequate operating conditions was done using the isotherm data and column configuration as given in Table 1. The intraparticle mass transfer rate constant k_p was chosen to be equal to 6 min^{-1}, so that $\alpha = 60$. The flow-rate ratios in sections 1 and 4 were fixed in accordance with the constraints given in Eqs. (27) and (30), which, for linear equilibria, may be re-written as:

$$\gamma_1 > \nu K_A = 1.5 \cdot 0.635 = 0.9525 \tag{33}$$

$$\gamma_4 < \nu K_B = 1.5 \cdot 0.314 = 0.471 \tag{34}$$

The values of γ_1 and γ_4 chosen for the optimization procedure were 1.5 and 0.155, respectively. For a rotation period of 3.3 min, this implies in SMB flow-rates of 18.5 and 8.55 ml/min in sections 1 and 4, respectively. Then, the area comprised by the triangle (0.471, 0.471); (0.9525, 0.9525); (0.471, 0.9525) was scanned by successive simulation and those values of γ_2 and γ_3 which resulted in greater purities than 99% for both extract and raffinate were kept to build the corresponding region of separation. This was done for $\alpha = 60$ and $\Omega = 0$, 1 and 2. Fig. 6 shows the areas of separation obtained as compared to that given in the frame of equilibrium theory. In the absence of non-equilibrium effects ($\Omega = 0$), the region of separation is similar to that obtained from the equilibrium theory. However, it is narrower since the number of mass transfer units is finite ($\alpha = 60$).

Table 2
SMB setup for simulations of chiral epoxide separation

Model parameters	Operating conditions	Columns
$Pe = 2000$	$T = 20°C$	$D_b = 2.6$ cm
$k_p = 24$ min^{-1}	Feed concentration = 5 g/l each	$L_b = 9.9$ cm
$\alpha = 160$	$t^* = 3.3$ min	Configuration: 2-2-2-2
$\Omega = 0, 1, 5, 10$	$Q_{Rec} = 21.38$ ml/min	Zone length = 19.8 cm
$\nu = 1.5$	$Q_E = 12.36$ ml/min	
	$Q_X = 8.64$ ml/min	
	$Q_{FEED} = 1$ ml/min	

As non-equilibrium effects are added (increasing Ω), the region of separation is reduced around the upper-mid portion of the $\gamma_2 = \gamma_3$ line. At the vicinity of this site, greater purities are obtained for all cases.

For the non-linear case, a similar strategy as described previously was applied. The column configuration and equilibrium isotherms used were those found in Table 2. The rotation period and flow-rates in sections 1 and 4 were calculated from retention time considerations and then checked against the constraints given in Eqs. (27) and (30). These constraints have been determined analytically for modified Langmuir isotherms in the frame of equilibrium theory by Mazzotti et al. [19].

The flow-rate in zone 1 is the greatest of all and may be determined by the equipment pressure drop limitations. We chose the value of 34 ml/min. In section 1, the strongly retained component A should be desorbed so that the solid ''leaves'' section 1 towards section 4 completely regenerated. Therefore, the rotation period should be larger than the retention time of component A so that there is enough time in a period for it to be washed out of the solid adsorbent. Fluid phase concentrations should be as low as possible so that only the linear portion of the modified Langmuir isotherm may be considered. Hence, the retention time of component A in zone 1 is:

$$t_{RA,1} = \frac{\epsilon V_b}{Q_1^*} \cdot [1 + \nu(K_A + b_A q_m)] \tag{35}$$

Using the values illustrated in Table 2 for column dimensions, phase ratio, equilibrium data and the assigned flow-rate of 34 ml/min, the column retention time of component A in zone 1 is 2.98 min. The rotation period was then set to 3.3 min, somewhat higher than the calculated retention time. With these values of rotation period and section 1 flow-rate, the flow-rate ratio γ_1 is equal to 4.3, which is greater than the minimum value of γ_1 as stated from the equilibrium theory:

$$\gamma_1 > \gamma_1^{min} = \nu(K_A + b_A q_m) = 3.81 \tag{36}$$

In section 4, the column retention time should be such that the less retained component is adsorbed and carried towards the raffinate port. In this section, the column retention time of component B may be written as:

$$t_{RB,4} = \frac{\epsilon V_b}{Q_4^*} \cdot \left[1 + \nu \frac{\Delta q_{B,F}^*}{\Delta C_{B,F}} \right] \tag{37}$$

where $\Delta q_{B,F}^*/\Delta C_{B,F}$ is the slope of the chord linking points $(C_{B,F}; q_{B,F}^*)$ to $(0, 0)$ with $C_A = 0$. Using the values given in Table 2, $C_{B,F} = 5$ g/l and hence $\Delta q_{B,F}^*/\Delta C_{B,F} = K_B + b_B q_m/(1 + b_B C_{B,F}) = 1.794$. Ideally, the column retention time of component B in section 4 should be greater than the rotation period, so that the its concentration front does not reach the end of the section and contaminate the eluent moving to section 1. Setting a value of $t_{RB,4} = 3.88$ min, Q_4^* is equal to 20 ml/min as calculated from Eq. (37). With these values, the flow-rate ratio γ_4 is 2.36, which is in accordance with the maximum value defined for this constraint (2.72). Although the derivation of the minimum bound on γ_4 is analytical, it requires some tedious calculations, which is out of the scope of this work and may be found elsewhere [19]

With these values of Q_1^*, Q_4^* and t^*, the corresponding flow-rate ratios in sections 1 and 4 are $\gamma_1 = 4.3$ and $\gamma_4 = 2.36$. By successive simulations, different values of γ_2 and γ_3 in the area defined by the equilibrium theory, with $\gamma_2 < \gamma_3$, were tested for
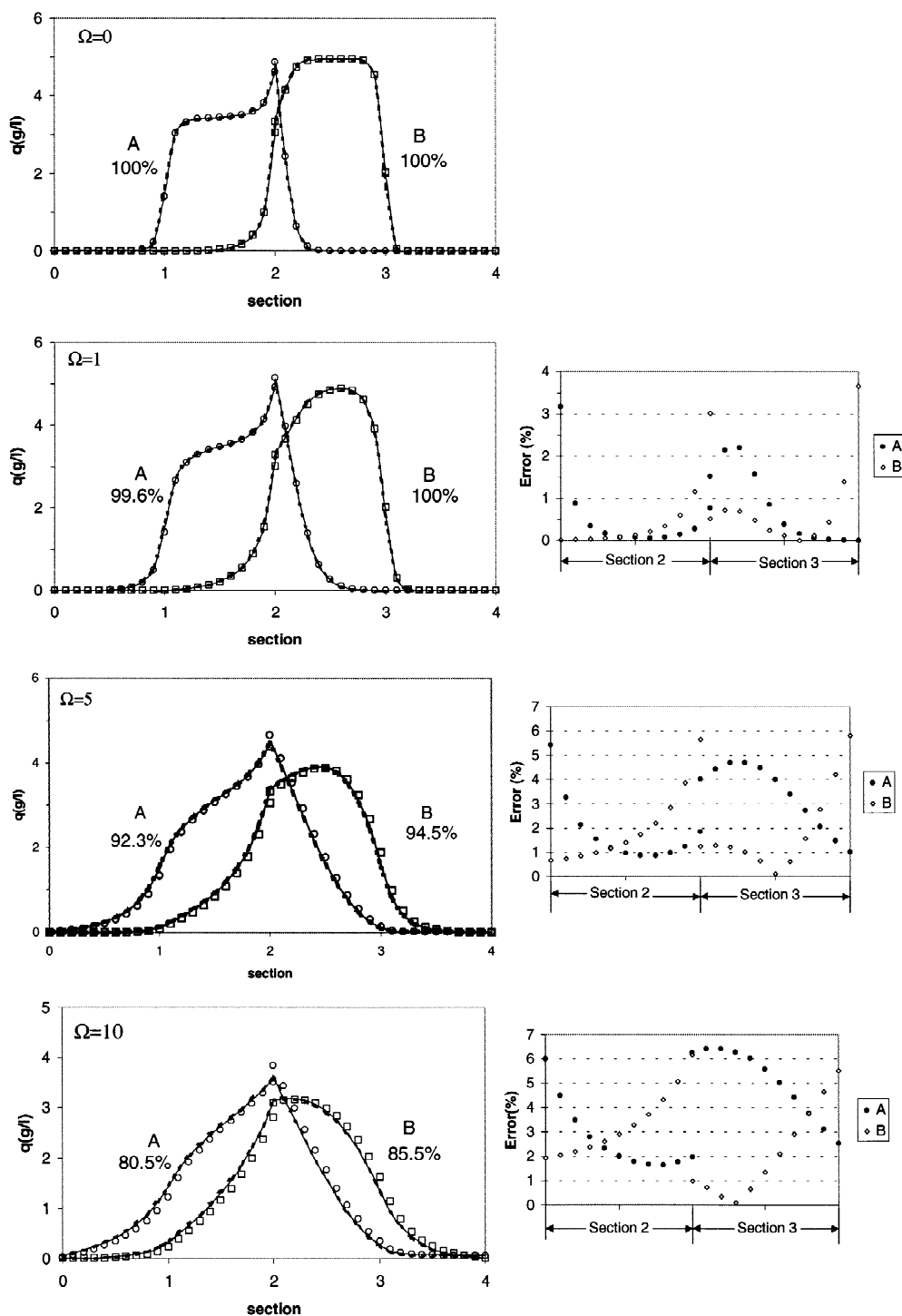
Fig. 4. Steady-state internal profiles for enantiomers A and B with $\alpha = 160$ and $\Omega = 0$, 0.1, 1 and 10. The dashed curves stand for the mean solid-phase concentration, $\bar{q}$; the continuous curves stand for surface concentration, q_s and the points stand for equilibrium surface concentration, q_s^* (circles for A and squares for B). The figures in each graph indicate extract purity (A) and raffinate purity (B).
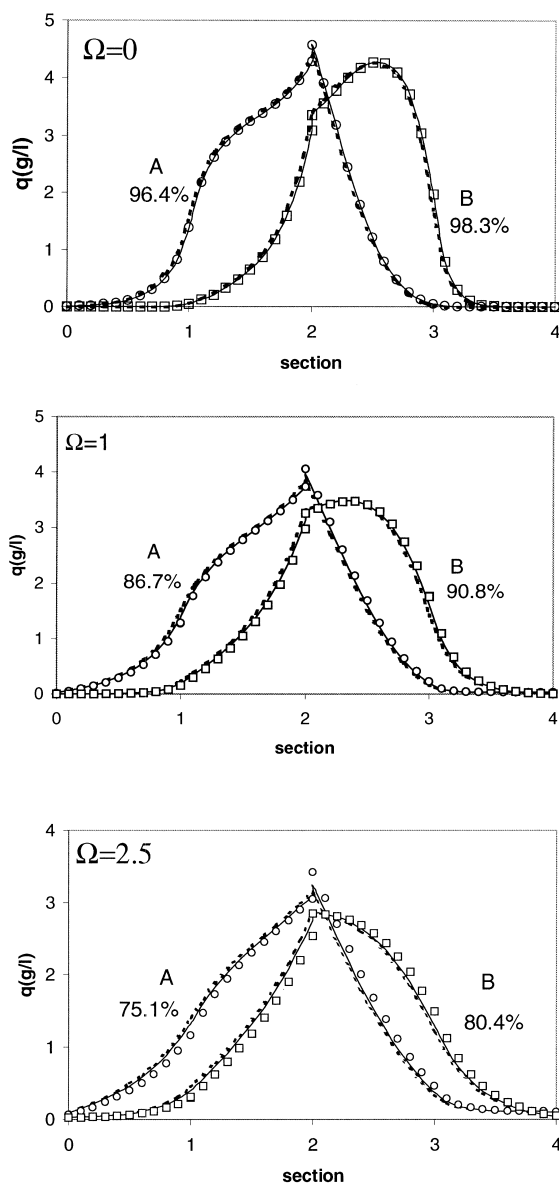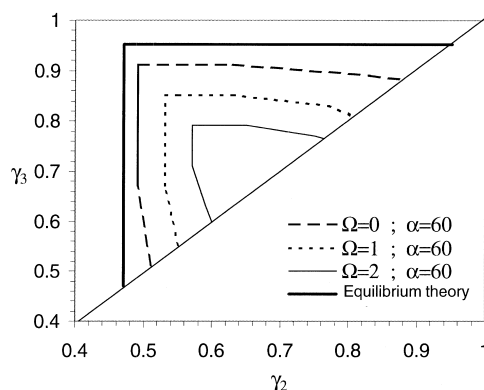
Fig. 6. Regions of separation in a $\gamma_2 \times \gamma_3$ plane for a SMB subject to non-equilibrium effects under linear equilibrium isotherms.

by comparing the region of separation as calculated analytically from the equilibrium theory [19] with that calculated for $\alpha = 160$ and $\Omega = 0$. In the other cases shown, the adsorption rate constant is arbitrarily decreased so as to obtain the values of $\Omega = 1$, 1.5 and 2. The major resistance to mass transfer in these cases is due to the non-equilibrium effects at the adsorbent particle interface. When Ω is small enough, the region of separation approaches that obtained in the frame of equilibrium theory. As the resistance to equilibrium attainment is increased, the region of separation disappears at Ω greater than 2. This suggests that care must be taken when designing SMB units to separations which may be subject to non-ideal equilibrium effects, e.g., high affinity

Fig. 5. Steady-state internal profiles for a SMB unit with $\alpha = 40$ and $\Omega = 0$, 0.1 and 1. Legends are the same as in Fig. 4.

the column configuration as given in Table 2 in order to find those values which result in both product purities higher than 99%. This was done for different situations of adsorption kinetics and is shown in Fig. 7. Note that the number of mass transfer units (α) is high enough so that equilibrium is nearly reached throughout the particle volume. This may be verified
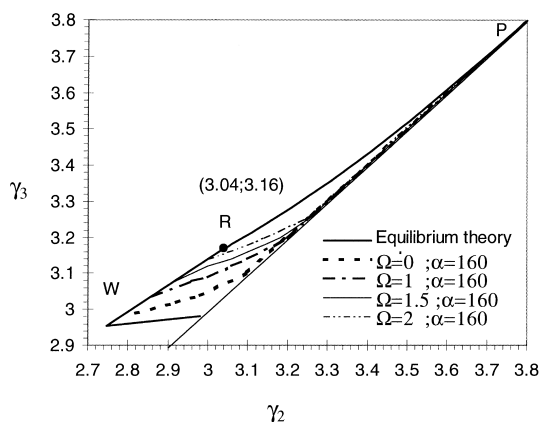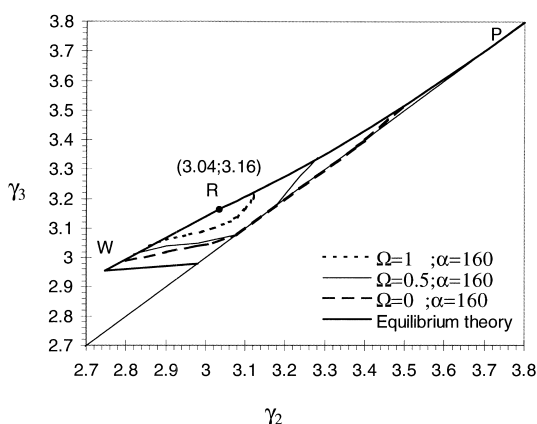

Fig. 7. Regions of separation in a $\gamma_2 \times \gamma_3$ plane for a SMB subject to non-equilibrium effects under non-linear equilibrium isotherms (linear + Langmuir) with $\gamma_1 = 4.3$ and $\gamma_4 = 2.14$.

solutes and/or steric effects present in stationary phase.

The same optimization procedure was performed again but with $\gamma_1 = 3.87$ and $\gamma_4 = 2.69$. These values are very close to the limiting values as predicted by the equilibrium theory (3.81 and 2.72, respectively). The corresponding regions of separation obtained for $\Omega = 0$, 0.5 and 1 are shown in Fig. 8. It is interesting to note that the regions of separation for the same Ω are different from those in Fig. 7. They tend to disappear at a lower Ω as compared to the previous case. Another interesting aspect to note is that, at $\Omega = 1$, the region of separation does not touch the $\gamma_2 = \gamma_3$ line, a different behavior from that observed in Fig. 7. This may be due to the proximity of γ_1 and γ_4 to the constraints given by the equilibrium theory. When mass transfer effects are present, these constraints are dependent on these effects and shift to new limits. This has been shown for SMB optimization of systems with linear equilibrium isotherms [18] and seems to apply to non-linear systems as well. Choosing γ_1 and γ_4 values as defined from the equilibrium theory may be an economic practice (minimum eluent requirement); however, this may lead to inadequate design when mass transfer/non-equilibrium effects are present and lower purities than expected may be obtained. Furthermore, the regions seem to converge to point "R", and as indicated in Fig. 8. In the building of the region of separation as stated in the equilibrium theory, the

segment WP is composed of a straight line (WR) and a curve (RP) which intersect at the converging point R. In the vicinity of this point, the highest average purities of both products have been observed for each of the cases simulated.

Fig. 9 illustrates the two trends observed for the regions of separation in linear and non-linear systems as non-equilibrium effects become important. In the linear case, the region of separation "shrinks" in relation to that given by the equilibrium theory from its upper-left corner towards the vicinity of $\gamma_2 = \gamma_3$ line. In the non-linear case, this "shrinking" effect of the region of separation in relation to that given by the equilibrium theory occurs in a different fashion. The regions of pure raffinate increase including the bottom of the "equilibrium triangle" while keeping the segment RP in common.

4. Conclusions

The effects of non-equilibrium adsorption kinetics on SMB performance were examined in this work for linear (glucose–fructose separation) and non-linear (chiral epoxide separation) isotherms. The concentration at the surface of the adsorbent particle was written out as a separate algebraic equation in the model using the assumption of equal rates of adsorption/desorption and intraparticle diffusion. For linear equilibrium systems, it was shown that the adsorption rate constant may be grouped with the intraparticle mass transfer rate constant so as to form an equivalent lumped rate constant. Therefore, as far as performance prediction is concerned, there is no need to distinguish non-equilibrium effects as a separate mechanism; however this may be useful if one intends to foresee the effects of particle size and temperature. In the non-linear case, it has been shown that, in spite of not obtaining large differences between the surface concentration and equilibrium solid-phase concentration in steady-state, the presence of non-equilibrium effects affects the performance of a SMB unit considerably. Especially when it comes to the prediction of flow-rate ratios which enhance separation (product purities above 99%), the inclusion of non-equilibrium effects is fundamental to a correct design of robust operating conditions, especially when dealing with high-affinity solutes

Fig. 8. Regions of separation in a $\gamma_2 \times \gamma_3$ plane for a SMB subject to non-equilibrium effects under non-linear equilibrium isotherms (linear + Langmuir) with $\gamma_1 = 3.87$ and $\gamma_4 = 2.69$.
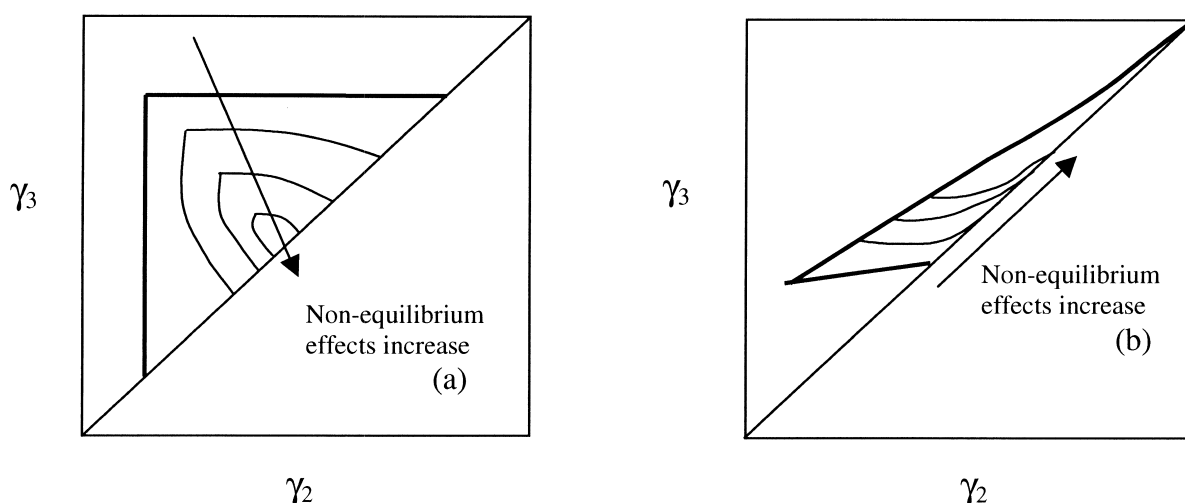
Fig. 9. Comparison of the regions of separation affected by adsorption/desorption kinetic effects for linear (a) and modified Langmuir (b) equilibrium isotherms.

and/or stationary phases with steric hindrances. The constraints on γ_1 and γ_4 must also be carefully chosen before performing a search for adequate SMB operating conditions since they are also affected by non-equilibrium effects.

5. Notation

b	parameter of the Langmuir isotherm (m^3/mol)
C	fluid phase concentration, mol/m^3 (void bed volume)
D_{ax}	axial dispersion coefficient, m^2/s
D_b	bed internal diameter, m
K	linear adsorption equilibrium constant (k_1/k_2)
k_1	adsorption rate constant, s^{-1}
k_2	desorption rate constant, s^{-1}
k_p	mass transfer rate constant as defined by the LDF approximation for diffusion in homogeneous solids, s^{-1}
L_b	bed length, m
L_j	zone length, m
Q	fluid phase flow-rate, m^3/s
Q^*	fluid phase flow-rate in SMB columns, m^3/s
$\bar{q}$	adsorbed phase concentration averaged

over the particle volume, mol/m^3 (particle)

q_m	maximum adsorption capacity as defined by the Langmuir isotherm, mol/m^3 (particle)
q_s	adsorbed phase concentration at the particle surface, mol/m^3 (particle)
q_s^*	theoretical adsorbed phase concentration as calculated from the equilibrium isotherm, mol/m^3 (particle)
t^*	SMB rotation period
$t_{Ri,j}$	retention time of component i in a column of section j
V_b	bed/column volume, m^3
U_F	interstitial fluid phase velocity, m/s
U_S	interstitial solid-phase velocity, m/s

5.1. Greek letters

α	number of particle mass transfer units
ϵ	bed void fraction
γ	ratio between fluid and solid-phases interstitial velocities
ν	phase ratio
Ω	ratio between intraparticle mass transfer rate constant and adsorption/desorption rate constant

5.2. Subscripts

1, 2, 3, 4	SMB/TMB zones
E	eluent
F	feed
i	refers to component
j	refers to SMB/TMB zone
REC	recycle
X	extract

Acknowledgements

References

[1] D.B. Broughton, C.G. Gerhold, US Pat. 2 985 589 (1961).
[2] D.B. Broughton, Chem. Eng. Prog. 64 (1968) 60.
[3] D.B. Broughton, R.W. Neuzil, J.M. Pharis, C.S. Brearley, Chem Eng. Prog. 66 (1970) 70.
[4] D.B. Broughton, Sep. Sci. Technol. 19 (1984) 723.
[5] J.A. Johnson, R.G. Kabza, in: G. Ganetsos, P.E. Barker (Eds.), Preparative and Production Scale Chromatography, Marcel Dekker, New York, 1993, Ch. 12, p. 257.
[6] R.-M. Nicoud, Simulated Moving Bed – Basics and Applications, Separex and ENSIC, INPL, Nancy, 1993.
[7] R.-M. Nicoud, Recent Advances in Industrial Chromatographic Processes, Novasep, Nancy, 1997.
[8] M.J. Gattuso, B. McCulloch, J.W. Priegnitz, in: Proceedings of the Chiral Europe '94 Symposium, 1994.
[9] M.J. Gattuso, B. McCulloch, D.W. House, W.M. Baumann, in: Proceedings of the Chiral USA '95 Symposium, 1995.
[10] M.J. Gattuso, B. McCulloch, D.W. House, W.M. Baumann, K. Gottschall, Pharm. Tech. Europe 8 (1996) 20.
[11] R.A. Sheldon, Chirotechnology – Industrial Synthesis of Optically Active Compounds, Marcel Dekker, New York, 1993.
[12] S.C. Stinson, Chem. Eng. News, September 27 (1993) 38.
[13] S.C. Stinson, Chem. Eng. News, September 19 (1994) 38.
[14] S.C. Stinson, Chem. Eng. News, July 17 (1995) 10.
[15] S.C. Stinson, Chem. Eng. News, October 9 (1995) 44.
[16] L.S. Pais, J.M. Loureiro, A.E. Rodrigues, J. Chromatogr. A 827 (1998) 215.
[17] L.S. Pais, J.M. Loureiro, A.E. Rodrigues, AIChE J. 44 (1998) 561.
[18] D.C.S. Azevedo, A.E. Rodrigues, AIChE J. 45 (1999) 956.
[19] M. Mazzotti, G. Storti, M. Morbidelli, J. Chromatogr. A 769 (1997) 3.
[20] T. Pröll, E. Küsters, J. Chromatogr. A 800 (1998) 135.
[21] B.B. Fish, R.W. Carr, R. Aris, AIChE J. 39 (1993) 1621.
[22] S. Lehoucq, A.V. Wouwer, E. Cavoy, in: F. Meunier (Ed.), Proceedings of FOA6, Elsevier, Amsterdam, 1998, p. 467.
[23] S. Swarup, G. Duan, C.B. Ching, in: F. Meunier (Ed.), Proceedings of FOA6, Elsevier, Amsterdam, 1998, p. 533.
[24] L.S. Pais, J.M. Loureiro, A.E. Rodrigues, J. Chromatogr. A 769 (1997) 25.
[25] E. Francotte, P. Richert, M. Mazzotti, M. Morbidelli, J. Chromatogr. A 796 (1998) 239.
[26] M. Juza, O. Di Giovanni, G. Biressi, V. Schurig, M. Mazzotti, M. Morbidelli, J. Chromatogr. A 813 (1998) 333.
[27] H.W. Dandekar, A.K. Chandhok, J.W. Priegnitz, in: M.D. LeVan (Ed.), Proceedings of the 5th Conference on Fundamentals of Adsorption, Elsevier, Amsterdam, 1996, p. 243.
[28] H. Koller, K.-H. Rimböck, A. Mannschreck, J. Chromatogr. 282 (1983) 89.
[29] G. Blaschke, J. Liq. Chromatogr. 9 (1986) 341.
[30] T. Shibata, I. Okamoto, K. Ishii, J. Liq. Chromatogr. 9 (1986) 313.
[31] E. Francotte, A. Junker-Buchheit, J. Chromatogr. A 576 (1992) 1.
[32] R.D. Whitley, K.E. Van Cott, N.-H.L. Wang, Ind. Eng. Chem. Res. 32 (1993) 149.
[33] A.E. Rodrigues, A.M.D. Ramos, J.M. Loureiro, M. Diaz, Z.P. Lu, Chem. Eng. Sci. 47 (1992) 4405.
[34] M.D. LeVan, in: F. Meunier (Ed.), Proceedings of FOA6, Elsevier, Amsterdam, 1998, p. 19.
[35] G. Bader, U.M. Ascher, SIAM J. Sci. Stat. Comput. 8 (1987) 483.
[36] U.M. Ascher, L.R. Petzold, J. Comp. Appl. Math. 43 (1992) 243.
[37] C.P. Leão, L.S. Pais, M. Santos, A.E. Rodrigues, in: J. Semel (Ed.), Process Identification in Practice, BHR Publication 28, 1997, p. 143.